RESILIENT INFRASTRUCTURE
June 1–4, 2016

PREDICTING FAILURE IN SLIDING ISOLATION BEARINGS UNDER LONG-PERIOD MOTIONS

Yu Bao
PhD Candidate, McMaster University, Canada

Tracy Becker
Assistant professor, McMaster University, Hamilton, Ontario, Canada

ABSTRACT

For the majority of structural systems, there has been a push to understand collapse behaviour and to quantify collapse margin ratios. However, for seismic isolation there is still significant work to be done in this area, especially for sliding bearings, for which little research on failure has been investigated. While it may be the goal of the designer that isolation bearing capacity is not reached, for performance based design it is essential to understand how and under what levels the bearing will fail. To investigate failure, a model based on the theory of rigid body kinematics, rigid body dynamics and contact mechanics is employed with an added parallel non-linear damper to explicitly consider the energy dissipation. Ricker pulses are extracted from long period motions and used to predict whether the bearing impacts and if that impact results in failure. The research finds that these pulses are good predictors providing that the extracted pulse periods are sufficiently long (greater than 0.5 s); otherwise the pulse does not dominate the response of the bearing. Generalized graphs are produced for use in predicting bearing performance and collapse margin ratio (assuming a rigid superstructure) at initial stages of design.

Keywords: Sliding isolation bearing; failure; pulse excitation; impact simulation; seismic isolation

1. INTRODUCTION

Seismic isolation has been widely accepted as one of the most effective way to mitigate seismic hazards and enhance the seismic performance of structures. Currently rubber and sliding bearings are the most commonly used isolation bearings and their mechanical behaviours have been widely studied in the literature. Even though seismic isolation has demonstrated its superiority over the traditional fixed-base design, there is still significant work to be done in this area, including understanding and predicting the failure mechanisms of isolated structures. Failure of isolated structure is an extremely complex phenomenon, which involves interaction between superstructure, isolation bearings and even the moat wall. The first step to address this critical issue is to look at the failure mechanism of a single isolation bearing.

For rubber bearings, shear failure and buckling failure are well understood (Kelly and Konstantinidis 2011). However, there is very little study on the failure mechanisms of sliding bearings. Sliding bearings consist of multiple components and its failure mechanism is highly dependent on the interaction between its components. Thus, a completely different failure mechanism is expected compared to rubber bearing.

In this paper a relative simple sliding bearing, known as double friction pendulum bearing (denoted as DFP hereafter), is used as an example to investigate the failure mechanism. Figure 1 illustrates the configuration of DFP, which is made up of a top plate, a rigid slider and a bottom plate, both plates have restraining rims to limit the displacement capacity of the bearing. The geometry parameters shown in Figure 1 are real design values used in Japan. When the DFP reaches its displacement limit, due to the presence of the restraining rims a couple develops from the restrainer reactions (as illustrated in Figure 2), resulting in yielding of the restraining rim, uplift of the supported mass or a combination of both. The uplift behaviour or yielding can lead to the failure of the DFP. The response of the DFP is investigated under Ricker pulse excitation, which is an approximation of original pulse-like

ground motions. It will be shown that using long period Ricker pulses to predict the failure of DFP provides a good approximation for time history analysis.

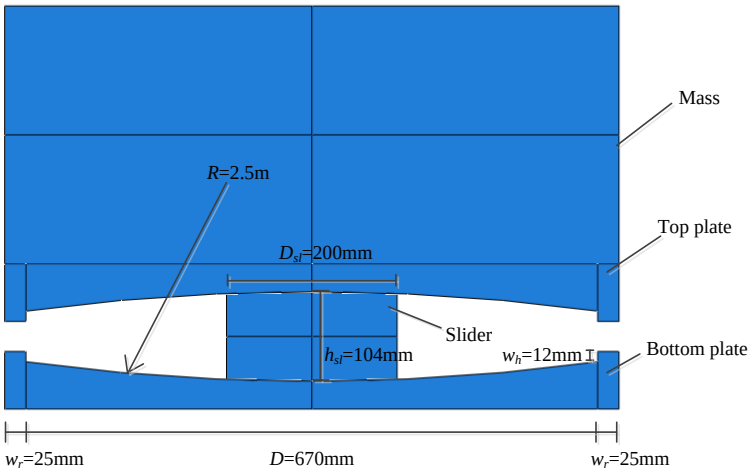

Figure 1: Double friction pendulum bearing configuration

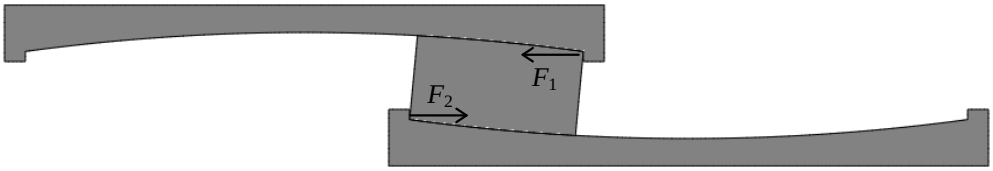

Figure 2: Illustration of restrainer forces

2. RIGID BODY MODEL

The rigid body model (Sarlis and Constantinou 2013) used for this study is based on the theory of rigid body kinematics, rigid body dynamics and contact mechanics. Each component of DFP is assumed to be rigid and their motions are measured at their centroids. For the bottom and top plate, only two translational degrees of freedom are considered, and for the slider, in addition to these two degrees of freedom, one rotational degree of freedom is also considered. All forces acting on the slider, including normal force, friction force and potential impact force, are assumed to concentrate on the four vertexes rather than distribute along the contact surface. Small penetrations are allowed between each component to generate the normal and impact force.

Being capable of simulating impact and uplift directly is the major advantage of this model. However, one drawback is that it does not account for energy dissipation during impact. This is because the original rigid body model employs a linear spring to model the impact. In order to address this issue, the Hertz's contact law with a nonlinear dashpot in parallel (Muthukumar and DesRoches 2006) is used to explicitly consider the energy dissipation. From the Hertz's contact law, the energy dissipation only occurs during the approaching phase and the impact force in this phase can be calculated from Eq.1, during the restitution phase there is no energy dissipation so the impact force is calculated from Eq.2.

[1] $$F(t) = k\delta(t)^{1.5} + c\dot{\delta}(t)$$

[2] $$F(t) = k\delta(t)^{1.5}$$

where k is the penalty stiffness, c is the damping coefficient and $\delta(t)$ is the penetration depth with time. The damping coefficient c can be approximated in terms of coefficient of restitution e (Jankowski 2005, 2006), as shown in Eq.3 and Eq.4.

[3] $$c = 2\xi\sqrt{k\sqrt{\delta(t)}\frac{m_1 m_2}{m_1 + m_2}}$$

[4] $$\xi = \frac{9\sqrt{5}\left(1-e^2\right)}{2e\left(e\left(9\pi-16\right)+16\right)}$$

where ξ is the damping ratio, m_1 and m_2 are masses of two colliding objects. The coefficient of restitution e indicates how much energy is dissipated during impact, e = 0 means all kinetic energy is dissipated while e = 1 means no energy is lost. For steel the coefficient of restitution e usually ranges from 0.4 to 0.7 (Jankowski 2010). In this study, the coefficient of restitution e is selected as 0.65 and it is found that this value gives a satisfactory estimation compared to finite element analysis.

2.1 Validation of rigid body model

The design parameters for this specific DFP studied in this paper are shown in Figure 1, the radius of curvature is 2.5 m and results in a second-slope period of the bearing T_b equals to 4.5 s. The friction coefficient μ is 0.05 and friction coefficient dependencies on velocity, pressure and temperature are ignored for simplicity.

The finite element model used for comparison is created in Abaqus/Standard. The steel is modelled with isotropic hardening to consider potential yielding of the restraining rims. The yield stress and the ultimate stress are 345 MPa and 450 MPa respectively, the ratio of post-yield stiffness to elastic stiffness is assumed as 0.01. The superstructure is represented by a mass block with rotational degree of freedom constrained.

Eleven pairs of Japanese ground motions are selected in this study to investigate the failure mechanism of the DFP and their information is listed in Table 1. The scaling methodology of these ground motions is described in FEMA P695, they are incremented by 0.01 g of pseudo acceleration at natural period *SA*(4.5 s).

Table 1: Eleven pairs of Japanese ground motions

Earthquake Number	Date	Event Name	Station	Magnitude
1	1995.01.17	Kobe, Japan	KJMA	6.9
2	1995.01.17	Kobe, Japan	Takatori	6.9
3	2000.10.06	Tottori, Japan	SMNH01	6.61
4	2000.10.06	Tottori, Japan	TTR08	6.61
5	2004.10.23	Niigata, Japan	NIG019	6.63
6	2004.10.23	Niigata, Japan	NIG021	6.63
7	2004.10.20	Niigata, Japan	NIGH11	6.63
8	2007.07.16	Niigata, Japan	NIG018	6.63
9	2008.06.14	Iwate, Japan	AKTH04	6.9
10	2008.06.14	Iwate, Japan	IWTH25	6.9
11	2008.06.14	Iwate, Japan	IWTH26	6.9

From finite element simulation results, two distinct failure mechanisms of DFP can be observed. One is caused by the significant yielding of the restraining rims, as shown in Figure 3 (left side figure), this failure mechanism happens when the superstructure mass is large (e.g. results in a slider pressure of 60 MPa). The other is caused by the uplift behaviour after the impact, as shown in Figure 3 (right side figure), and this phenomenon usually happens when superstructure mass is small (e.g. results in a slider pressure of 10 MPa). In this study since usually DFP is under high pressure, a slider pressure of 60 MPa is used to represent the superstructure mass.

The rigid body model is capable of capturing the failure mechanism due to uplift but inherently impossible to simulate the yielding behaviour with the rigid body assumption. Previous study (Bao et al. 2015) found this rigid body model provides a good estimation of critical pseudo acceleration values when failure mechanism is due to uplift (i.e. small superstructure mass). When the failure mechanism is due to yielding rather than uplift, the rigid

body model still provides a satisfactory prediction of critical pseudo acceleration values compared to finite element analysis results, as shown in Figure 4.

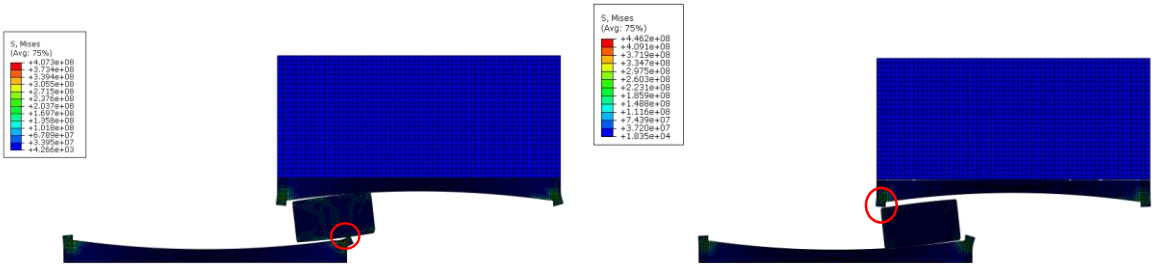

Figure 3: Two failure mechanisms of DFP (left side: due to yielding, right side: due to uplift)

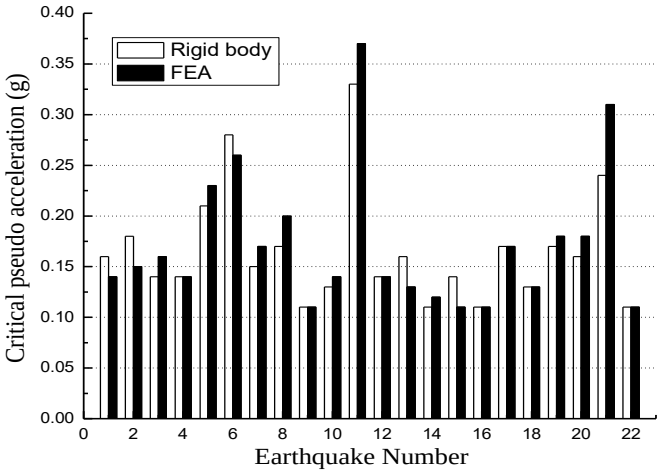

Figure 4: Comparison of critical pseudo acceleration between finite element model and rigid body model

3. FAILURE OF DOUBLE FRICTION PENDULUM BEARING UNDER PULSE EXCITATIONS

In this section the failure of DFP is studied under analytical pulse excitations. Compared to the highly variable ground motions, analytical pulses usually have a simple expression with several parameters which have clear physical meanings.

There are many different kinds of analytical pulses existing in the literature (Mavroeidis and Papageorgiou 2003). In this study Ricker pulses (Ricker 1943, 1944) are selected as the input excitation. Ricker pulses have symmetric and antisymmetric forms, which are expressed in Eq.5 and Eq.6 respectively.

[5] $$\ddot{g}(t) = A_p\left(1-\frac{2\pi^2 t^2}{T_p^2}\right)e^{-\frac{\pi^2 t^2}{T_p^2}}$$

[6] $$\ddot{g}(t) = \frac{A_p}{1.38}\left(\frac{4\pi^2 t^2}{3T_p^2}-3\right)\frac{2\pi t}{\sqrt{3}T_p}e^{-\frac{2\pi^2 t^2}{3T_p^2}}$$

where A_p is the amplitude of Ricker pulse and T_p is the period. Figure 5 shows the shapes of symmetric and antisymmetric Ricker pulse with an amplitude of 0.8 g and a period of 0.5 s.

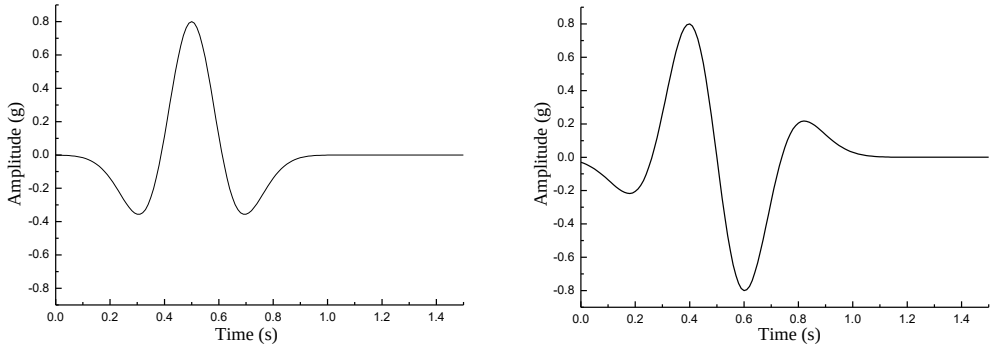

Figure 5: Symmetric and antisymmetric Ricker pulse

3.1 Maximum impact velocity spectrum

The impact velocity spectrum (Davis 1992) is used to describe the response of DFP under one specific Ricker pulse using the rigid body model. In this spectrum, the horizontal coordinate represents the ratio of the bearing period T_b (i.e. 4.5 s in this study) to the pulse period T_p, the vertical coordinate represents velocity of top plate relative to bottom plate at every occurrence of impact. Figure 6 shows the impact velocity spectra for symmetric and antisymmetric Ricker pulses with the same amplitude A_p =0.8 g but varying periods, note the pulse period T_p is limited to 7.5 s because longer period pulse is not realistic. Each dot indicates a single impact event and the cross symbol means failure due to uplift has occurred. From the impact velocity spectra it is observed that during one specific Ricker pulse excitation, DFP may experience multiple impact events, but only the impact with the maximum relative velocity required to lead to failure. Since we are primarily interested in predicting failure, only the maximum impact velocity is required. Thus the maximum impact velocity spectrum can be constructed, as shown by the line in Figure 6. Figure 7 shows the maximum impact velocity spectra when with increasing Ricker pulse amplitudes, similarly the cross symbol indicates failure occurs.

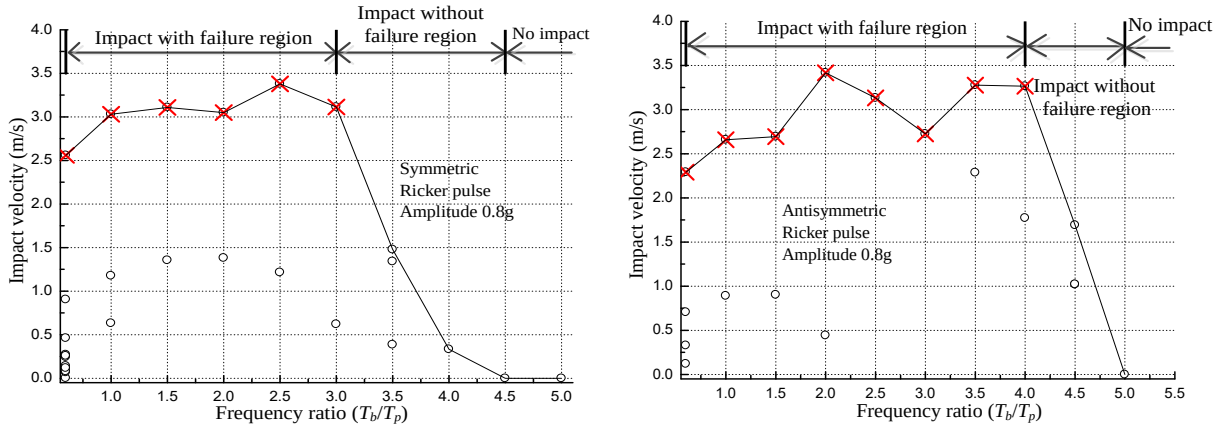

Figure 6: Impact velocity spectra for symmetric and antisymmetric Ricker pulses

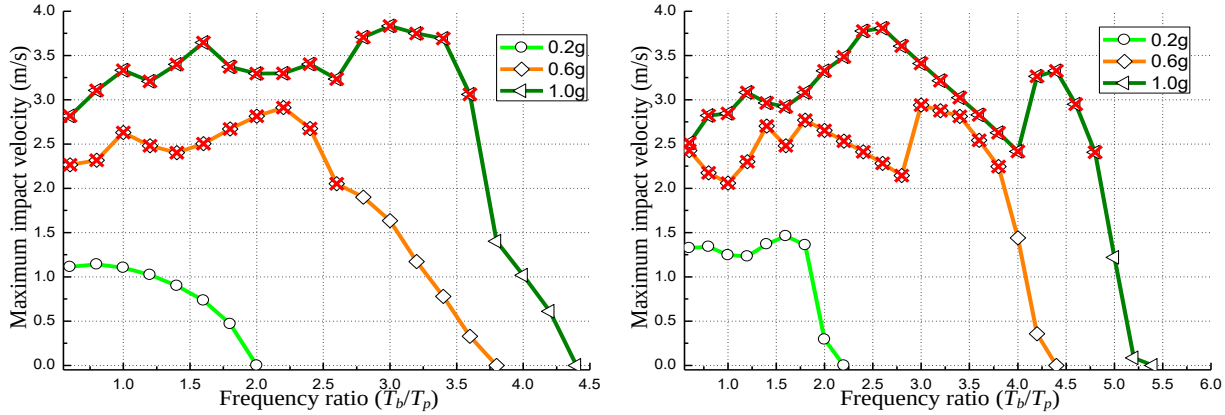

Figure 7: Maximum impact velocity spectra with different amplitudes (left: symmetric, right: antisymmetric)

3.2 Impact region spectrum

Looking at the maximum impact velocity spectra again, it is observed that given a specific amplitude of the Ricker pulse, the frequency ratio can be divided into three regions based on the final status of the DFP: impact with failure region, impact without failure region and no impact region, as illustrated in Figure 6.

Based on this feature, the impact region spectrum can be constructed from the maximum impact velocity spectrum as shown in Figure 8, which directly describes the final status of the DFP given a combination of the amplitude and period of Ricker pulses. The impact region spectrum is useful for the preliminary design of isolated structures and seismic performance evaluation.

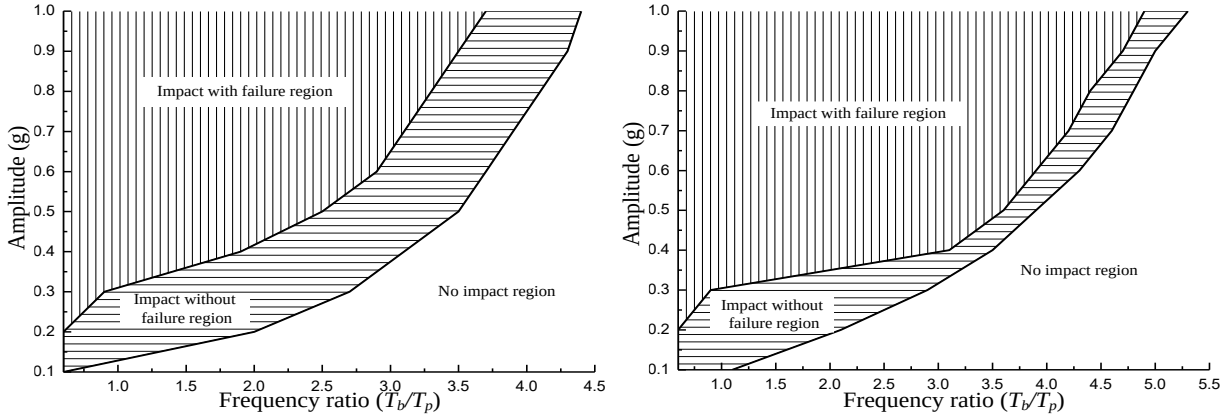

Figure 8: Impact region spectra (left: symmetric, right: antisymmetric)

4. FAILURE PREDICTION FOR JAPANESE GROUND MOTIONS

In this section, the impact region spectra will be used to predict the critical pseudo acceleration values for Japanese ground motions. In order to use the impact region spectrum, analytical Ricker pulses must be determined from Japanese ground motions, which requires the wavelet analysis.

4.1 Wavelet analysis of Japanese ground motions

Wavelet analysis has been applied to ground motions either to determine whether it can be classified as pulse-like (Baker 2007) or estimate its pulse parameters (Vassiliou and Makris 2011). In this study the methodology proposed by Vassiliou and Makris will be used to determine the Ricker pulse parameters for Japanese ground motions. In their methodology, three different weighting functions: $w(s) = 1/\sqrt{s}$, $w(s) = 1/s$, $w(s) = 1$ are used to perform the following integral in Eq.7 to extract the wavelet from ground motion.

[7] $$C(s,\xi) = w(s)\int_{-\infty}^{+\infty} \ddot{u}_g(t)\psi\left(\frac{t-\xi}{s}\right)dt$$

where $\psi(\bullet)$ is the mother wavelet function, which is the Ricker pulse in this study, s and ξ are constants that control the dilation and translation of the mother wavelet. Note in Eq.7 the wavelet analysis is applied to acceleration records, but it is also applicable to velocity records. Figure 9 and Figure 10 show the extracted Ricker pulses for one sample Japanese ground motion when applying weighting function $w(s) = 1/s$ to acceleration and velocity records respectively. In both figures, the symmetric and antisymmetric annotations are in terms of the acceleration pulses rather than the velocity pulses. For this motion it is clear that extracting the Ricker pulse from the velocity record provides a better representation of the ground motion.

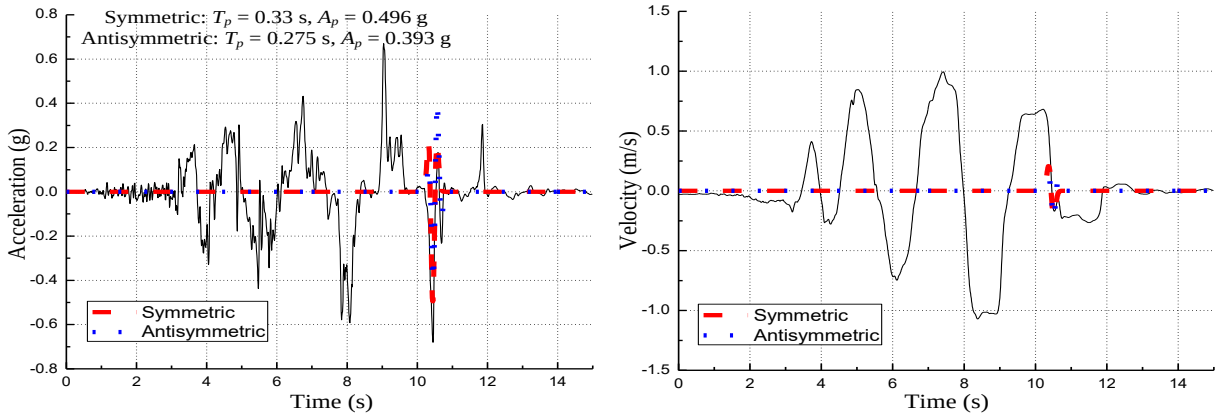

Figure 9: Extracted pulses from acceleration record (left: extracted Ricker pulses, right: corresponding velocities)

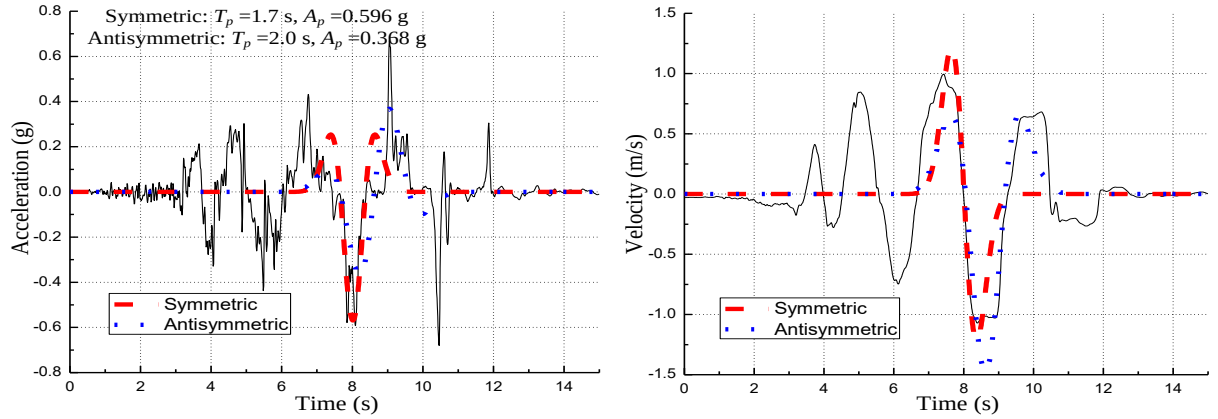

Figure 10: Extracted pulses from velocity record (left: corresponding Ricker pulses, right: extracted velocities)

Two indexes, the acceleration index e_a and the velocity index e_v (Vassiliou and Makris 2011), are used to evaluate to what extent the extracted Ricker pulses are matched with the original ground motions, their mathematical expressions are defined in Eq.8 and Eq.9.

[8] $$e_a = \frac{\int_{-\infty}^{+\infty} \ddot{u}_g(t)\ddot{u}_p(t)dt}{\int_{-\infty}^{+\infty}\left[\ddot{u}_g(t)\right]^2 dt}$$

[9] $$e_v = \frac{\int_{-\infty}^{+\infty} \dot{u}_g(t)\dot{u}_p(t)dt}{\int_{-\infty}^{+\infty}\left[\dot{u}_g(t)\right]^2 dt}$$

where subscript g denotes original ground motion and subscript p denotes extracted Ricker pulse. Then there are four criteria to determine the best match Ricker pulses:

1. Ricker pulse directly extracted from acceleration history that corresponds to the maximum acceleration index e_a.
2. Ricker pulse directly extracted from acceleration history that corresponds to the maximum velocity index e_v.
3. Ricker pulse derived from velocity history that corresponds to the maximum acceleration index e_a.
4. Ricker pulse derived from velocity history that corresponds to the maximum velocity index e_v.

Previous study (Bao et al. 2015) found that criterion No.3 gives the best prediction for 14 pairs of pulse-like ground motions recommended by FEMA P695. But in this study, it is found criterion No.4 provides the best estimation, this phenomenon will be discussed in the subsequent section. For comparison purpose, both prediction results from criteria No.3 and No.4 will be provided in the following section.

4.2 Prediction of critical pseudo acceleration

With the best match Ricker pulse determined for ground motion and the impact region spectrum, it is easy to predict the critical pseudo acceleration value $SA(T_b)$ which leads to failure of the DFP. To illustrate this procedure, the sample Japanese ground motion is used again. For this motion, it is coincidental that the best match Ricker pulse is an antisymmetric Ricker pulse with amplitude A_p = 0.305 g and period T_p = 2.325 s regardless of which criterion is used. This motion is then scaled up in accordance with FEMA P695 with an increment of 0.01g. Every time the motion is scaled, the amplitude A_p associated with the best match pulse is scaled and plotted with the impact region spectrum to determine whether failure occurs. Figure 11 shows this procedure: when the sample ground motion is scaled to $SA(T_b)$ = 0.15 g, the best match Ricker pulse has an amplitude A_p = 0.342 g (and period T_p = 2.325 s), after it is plotted on the impact region spectrum, we can see it locates in the impact without failure region. Similarly, when ground motion is scaled up to $SA(T_b)$ = 0.16 g, the best match Ricker pulse has an amplitude A_p = 0.365 g (and period T_p = 2.325 s), this time we find it locates in the impact with failure region. Therefore the predicted critical pseudo acceleration value for this sample Japanese ground motion is 0.16 g. From time history analysis using rigid body model, the actual value is 0.14 g.

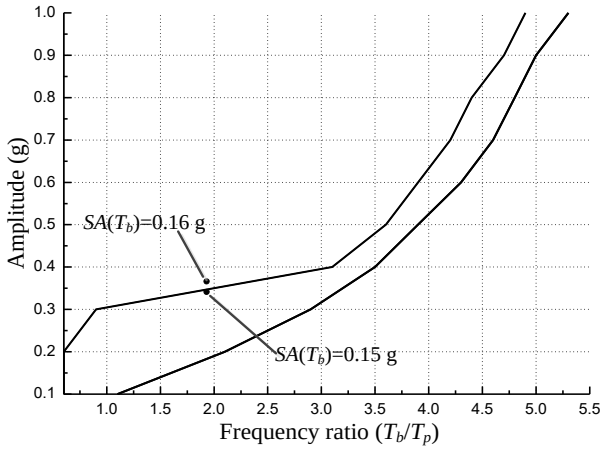

Figure 11: Critical pseudo acceleration $SA(T_b)$ prediction for sample Japanese ground motion

Figure 12 compares the predicted values with the actual pseudo acceleration values for different selection criterion. It is obvious that the prediction results from criterion No.4 is better than the prediction made from criterion No.3. As mentioned earlier, with the FEMA 14 pairs of pulse-like ground motions, it is criterion No.3 provides a better prediction. The authors believe that the inconsistent conclusion can be explained by the best match pulses selected. Criterion No.3 results in more short period pulses when applied to the Japanese motions as some of the motion did not have significant pulse contributions. To look into this, the prediction results are categorized into two groups based on the period of the best match Ricker pulse. It is proposed that pulses with a period longer than 0.5 s should be deemed as long period. Table 2 below shows statistical analysis results for predicted values. Prediction results are

defined as good if the predicted values are within 20% of the actual values. When the best match Ricker pulse is identified as long period pulse, the Ricker pulse usually provides a good estimation. This observation is in accordance with the result from the FEMA 14 pairs of pulse-like ground motions. Under what conditions the contribution of the long period pulse dominates the response of the DFP is a topic for future research.

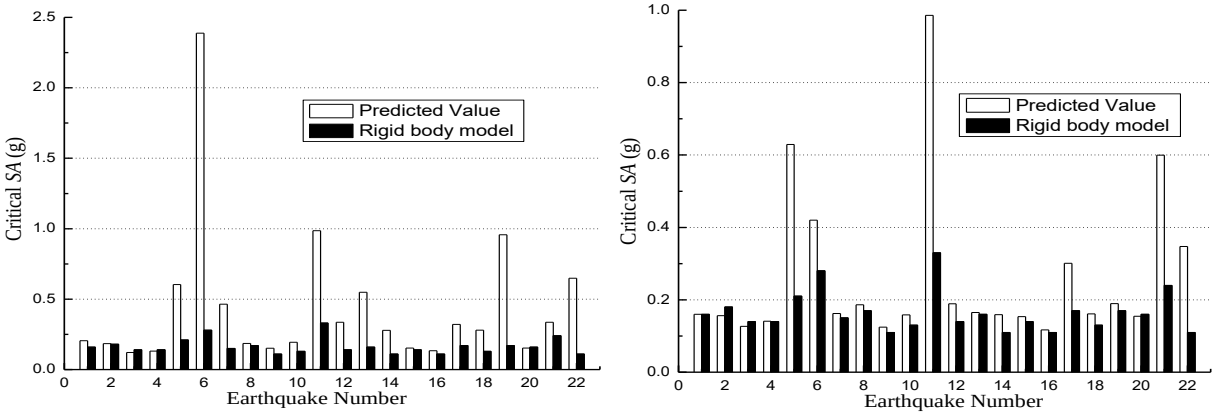

Figure 12: Comparison of predicted and actual pseudo acceleration values (left: criterion No.3, right: criterion No.4)

Table 2: Summary of ground motion prediction results

Selection criterion	Good estimation /Total	Good estimation (T_p≥0.5 s) /Total	Good prediction (T_p<0.5s) /Total
No.3	8/22	8/12	0/10
No.4	14/22	13/18	1/4

5. CONCLUSIONS

In this paper, the response of DFP is analyzed when it reaches its physical displacement limit. From detailed finite element analysis, two failure mechanisms are observed. A rigid body model capable of capturing the uplift failure mechanism is used. It is found even though it cannot capture yielding, it still provides a very good prediction in terms of pseudo accelerations. The response of DFP under analytical Ricker pulses are studied, in order to describe the behaviour of DFP, the impact region spectrum is developed. With the impact region spectrum and performing wavelet analysis to Japanese ground motions, it is able to predict the critical pseudo accelerations. It is found that usually long period Ricker pulse will dominate the response of DFP and thus gives a good estimation compared to short period Ricker pulse.

ACKNOWLEDGEMENTS

The authors would like to express gratitude to Mr. Hiroki Hamaguchi of the Takenaka R&D Institute for providing the design parameters of the double friction pendulum bearing and the Japanese ground motions used in this study. The invaluable comments and suggestions from Mr. Hiroki Hamaguchi, Dr. Masashi Yamamoto and Dr. Masahiko Higashino of the Takenaka R&D Institute are also gratefully acknowledged.

REFERENCES

Applied Technology Council. 2009. *FEMA P695: Quantification of building seismic performance factors*. Washington D.C., USA.

Baker, J.W. 2007. Quantitative classification of near-fault ground motions using wavelet analysis. *Bulletin of the seismological society of America* , 97(5):1486-1501.

Bao, Y, Becker, T.C and Hamaguchi, H. 2015. Failure of double friction pendulum bearings under pulse-type motions. *Earthquake Engineering and Structural Dynamics* (in review).

Davis, R.O. 1992. Pounding of buildings modelled by an impact oscillator. *Earthquake engineering and structural dynamics*, 21:253-274.

Jankowski, R 2005. Non-linear viscoelastic modelling of earthquake-induced structural pounding. *Earthquake Engineering and Structural Dynamics*, 34:595-611.

Jankowski, R 2006. Analytical expression between the impact damping ratio and the coefficient of restitution in the non-linear viscoelastic model of structural pounding. *Earthquake Engineering and Structural Dynamics*, 35:517-524.

Jankowski, R 2010. Experimental study on earthquake-induced pounding between structural elements made of different building materials. *Earthquake Engineering and Structural Dynamics*, 39:343-354.

Kelly, J.M and Konstantinidis, D. 2011. *Mechanics of Rubber Bearings for Seismic and Vibration Isolation*, John Wiley & Sons Ltd, Chichester, UK.

Mavroeidis, G.P, Papageorgiou, A.S. 2003. A mathematical representation of near-fault ground motions. *Bulletin of the seismological society of America*, 93(3):1099-1131.

Muthukumar, S, DesRoches, R. 2006. A Hertz contact model with non-linear damping for pounding simulation. *Earthquake Engineering and Structural Dynamics*, 35:811-828.

Ricker, N. 1944. Wavelet functions and their polynomials. *Geophysics*, 9:314-323.

Ricker, N. 1943. Further developments in the wavelet theory of seismogram structure. *Bulletin of the seismological society of America*, 33:197-228.

Sarlis, A.A and Constantinou, M.C. 2013. *Model of triple friction pendulum bearing for general geometric and frictional parameters and for uplift conditions*, technical report MCEER-13-0010, Buffalo, NY, USA.

Vassiliou, M.F, Makris, N. 2011. Estimating time scales and length scales in pulselike earthquake acceleration records with wavelet analysis. *Bulletin of the seismological society of America*, 101(2):596-618.